NASA/CR—2010-216229

Microstructure Modeling of 3rd Generation Disk Alloys

Second Annual Report

Herng-Jeng Jou
QuesTek Innovations LLC, Evanston, Illinois

March 2010

NASA STI Program . . . in Profile

Since its founding, NASA has been dedicated to the advancement of aeronautics and space science. The NASA Scientific and Technical Information (STI) program plays a key part in helping NASA maintain this important role.

The NASA STI Program operates under the auspices of the Agency Chief Information Officer. It collects, organizes, provides for archiving, and disseminates NASA's STI. The NASA STI program provides access to the NASA Aeronautics and Space Database and its public interface, the NASA Technical Reports Server, thus providing one of the largest collections of aeronautical and space science STI in the world. Results are published in both non-NASA channels and by NASA in the NASA STI Report Series, which includes the following report types:

- TECHNICAL PUBLICATION. Reports of completed research or a major significant phase of research that present the results of NASA programs and include extensive data or theoretical analysis. Includes compilations of significant scientific and technical data and information deemed to be of continuing reference value. NASA counterpart of peer-reviewed formal professional papers but has less stringent limitations on manuscript length and extent of graphic presentations.

- TECHNICAL MEMORANDUM. Scientific and technical findings that are preliminary or of specialized interest, e.g., quick release reports, working papers, and bibliographies that contain minimal annotation. Does not contain extensive analysis.

- CONTRACTOR REPORT. Scientific and technical findings by NASA-sponsored contractors and grantees.

- CONFERENCE PUBLICATION. Collected papers from scientific and technical conferences, symposia, seminars, or other meetings sponsored or cosponsored by NASA.

- SPECIAL PUBLICATION. Scientific, technical, or historical information from NASA programs, projects, and missions, often concerned with subjects having substantial public interest.

- TECHNICAL TRANSLATION. English-language translations of foreign scientific and technical material pertinent to NASA's mission.

Specialized services also include creating custom thesauri, building customized databases, organizing and publishing research results.

For more information about the NASA STI program, see the following:

- Access the NASA STI program home page at *http://www.sti.nasa.gov*

- E-mail your question via the Internet to *help@sti.nasa.gov*

- Fax your question to the NASA STI Help Desk at 443–757–5803

- Telephone the NASA STI Help Desk at 443–757–5802

- Write to:
  NASA Center for AeroSpace Information (CASI)
  7115 Standard Drive
  Hanover, MD 21076–1320

NASA/CR—2010-216229

Microstructure Modeling of 3rd Generation Disk Alloys

Second Annual Report

Herng-Jeng Jou
QuesTek Innovations LLC, Evanston, Illinois

Prepared under Contract NNC07CB01C

National Aeronautics and
Space Administration

Glenn Research Center
Cleveland, Ohio 44135

March 2010

Level of Review: This material has been technically reviewed by NASA technical management.

Available from

NASA Center for Aerospace Information
7115 Standard Drive
Hanover, MD 21076–1320

National Technical Information Service
5301 Shawnee Road
Alexandria, VA 22312

Available electronically at http://gltrs.grc.nasa.gov

CONTENTS

EXECUTIVE SUMMARY

The objective of this program is to model, validate, and predict the precipitation microstructure evolution, using *PrecipiCalc*® software, for 3rd generation Ni-based gas turbine disc superalloys during processing and service, with a set of logical and consistent experiments and characterizations. Furthermore, within this program, the originally research-oriented microstructure simulation tool will be further improved and implemented to be a useful and user-friendly engineering tool.

In this report, the key accomplishment achieved during the second year (2008) of the program is summarized. The activities of this year include final selection of multicomponent thermodynamics and mobility databases, precipitate surface energy determination from nucleation experiments, multiscale comparison of predicted versus measured intragrain precipitation microstructure in quench samples showing good agreement, isothermal coarsening experiments and interaction of grain boundary and intergrain precipitates, primary γ' microstructure of subsolvus treatment, and finally the software implementation plan for the third year of the project.

In the following year, the calibrated models and simulation tools will be validated against an independently developed experimental data set, with actual disc heat treatment process conditions. Furthermore, software integration and implementation will be developed to provide material engineers valuable information in order to optimize the processing of the 3rd generation gas turbine disc alloys.

Microstructure Modeling of 3rd Generation Disk Alloys
Second Annual Report

Herng-Jeng Jou
QuesTek Innovations LLC
Evanston, Illinois 60201

Introduction

The predictive science-based computational materials modeling and tools have a great potential to accelerate the process optimization of the 3rd generation Ni-base superalloys in gas turbine disc applications. By extending the DARPA-AIM methodology, previously demonstrated in disc alloys IN100 and R88DT[1,2], this NASA Aviation Safety Program is aiming to establish logical calibration, validation and user-friendly implementation of *PrecipiCalc*®, a multicomponent multiphase precipitation simulation software, for four 3rd generation nickel-based disk superalloys: ME3 (also called René104), LSHR (Low-Solvus, High-Refractory alloys developed by NASA), Alloy 10 (developed by Honeywell), and RR1000 (developed by Rolls-Royce). The nominal compositions are listed in Table 1.

Table 1. Nominal compositions of the four 3rd generation disc alloys, in wt%, studied under this program.

wt%	Ni	Cr	Co	Mo	W	Al	Ti	Nb	Ta	Hf	C	B	Zr
ME3	Bal.	13.1	20.0	3.8	1.9	3.5	3.6	1.1	2.3	–	0.040	0.030	0.05
LSHR	Bal.	13.0	21.0	2.7	4.3	3.5	3.5	1.5	1.6	–	0.030	0.030	0.05
Alloy10	Bal.	10.2	14.9	2.7	6.2	3.7	3.9	1.9	0.9	–	0.030	0.030	0.10
RR1000	Bal.	15.0	18.5	5.0	–	3.0	3.6	–	2.0	0.5	0.027	0.015	0.06

The program is on schedule for this reporting period. The major activities conducted in 2008 and a draft project plan for 2009 are shown in the Gantt chart (see Figure 1). The project team includes NASA Glenn Research Center (GRC), QuesTek, AFRL (as scientific advisor), Rolls-Royce (as industrial advisor), and University of Cambridge. Regular monthly teleconferences among the project team and monthly reports were facilitated to enhance communication. Furthermore, the results of this project were presented at the Superalloys 2008 conference by QuesTek's Gregory Olson, and also published in the proceeding, titled "Precipitation Model Validation in 3rd Generation Aeroturbine Disc Alloys" authored by QuesTek and NASA GRC's engineers.

The main activities in 2008 are Task 2 — Development of Calibration and Validation Data, and Task 3 — γ' Precipitation Modeling, although we spent some effort to finalize Task 1 — Fundamental Multicomponent Models, and started Task 5 — Software Implementation and Dissemination. Hence, this report will summarize the results and progress in Tasks 1, 2, 3 and 5 in the following sections.

The 2009 plan in Figure 1 is only preliminary as further planning on the carbide microstructure (part of Task 4 — Precipitation Modeling for Embrittling Phases) and validation with heat treated samples will be established in early 2009 and the 2009 plan (including Task 6 — Microstructure Variation and Optimization) will be further developed.

[1] H.-J. Jou, P. Voorhees and G.B. Olson, "Computer Simulations for the Prediction of Microstructure/Property Variation in Aeroturbine Disks," *Superalloys 2004*, Eds K.A. Green, T.M. Pollock, H. Harada, T.E. Howson, R.C. Reed, J.J. Schirra, and S. Walston, 2004, 877-886.
[2] A.M. Wusatowska-Sarnek, G. Ghosh, G.B. Olson, M.J. Blackburn, and M. Aindow, "A Characterization of the Microstructure and Phase Equilibria Calculations for the Powder Metallurgy Superalloy IN100," *J. Materials Research*, 18 (2003), 2653-2663.

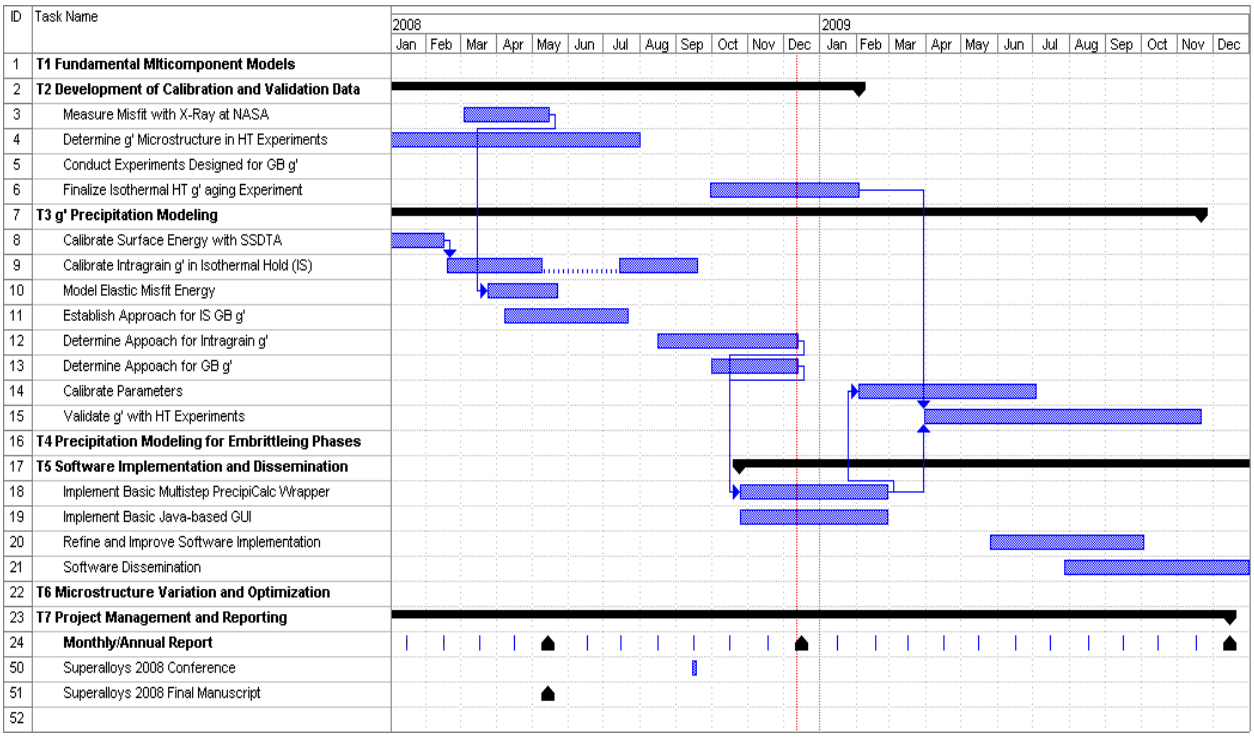

Figure 1. Gantt chart of the program

Development of *PrecipiCalc* Calibration and Validation Protocol and Task 2 — Development of Calibration and Validation Data

Table 2. *PrecipiCalc* calibration and validation protocol.

Experiments	CALPHAD Fundamental Databases	Material Kinetic Model Parameters
Equilibrium Age + APT and EDS Compositions	Thermodynamics, ΔE	
Diffusion Couple + Microanalysis	Mobility, D_{scale}	
SSDTA + APT		σ_{coh}, G_{el} (est.)
(1) Coarsening Age + SEM/TEM for γ' size and fraction (2) Subsolvus Solution Treatment + Controlled Cooling		σ_{incoh}, M_O
XRD, TEM for misfit	Molar Volume	G_{el}, $R_{coh \rightarrow incoh}$

To achieve a successful *PrecipiCalc* model calibration and validation for γ' microstructure prediction, a standard *PrecipiCalc* calibration and validation protocol for intragranular γ' precipitation was developed and shown in Table 2. This protocol employs independent experimental measurements to decouple and/or minimize the cross interaction between model parameters, allowing the determination

of the model parameters with high fidelity and minimum overfitting. The protocol also sequentially addresses the foundational databases and model parameters of the *PrecipiCalc* method, which include:

- CALPHAD fundamental databases — *PrecipiCalc* relies on CALPHAD-based databases to capture fundamental mechanistic features of multicomponent alloys. These databases and associated tuning parameters include:
    - Thermo-Calc®[3] compatible thermodynamic databases — representing bulk free energy with state variables such as composition and temperature;
    - ΔE — a phase free energy shift in Thermo-Calc to locally tune equilibrium phase fractions;
    - DICTRA[4] compatible mobility databases — representing atomic mobility and allowing calculation of diffusivity when combined with the thermodynamic database;
    - D_{scale} — diffusivity correction factor used by *PrecipiCalc* to easily rescale the diffusivity matrix for local fitting;
    - Molar Volume — preliminary multicomponent molar volume models were developed for both γ and γ' under the AIM program
- Material kinetic model parameters:
    - σ_{coh} — coherent surface energy, which is the key parameter affecting the nucleation barrier when particles are small and coherent with the surrounding matrix;
    - G_{el} — elastic coherency (misfit) energy adds additional energy penalty to the precipitation when the particles are coherent with the matrix;
    - σ_{incoh} — incoherent surface energy captures the increased surface energy when the particles lose coherency with the matrix;
    - M_o — prefactor for the interfacial mobility term to describe incoherent interfaces, while the corresponding activation energy is scaled to that for solvent self diffusion;
    - $R_{coh \rightarrow incoh}$ — the characteristic particle size for coherency transition.

Following the established protocol, high-temperature long aging is applied to Ni-based superalloys to produce near equilibrium microstructures, and matrix/particle compositions are measured by APT (Atom Probe Tomography) and EDS (Electron Dispersion Spectroscopy). The results help down-select a candidate thermodynamic database and determine potential simple energy corrections ΔE. Next, diffusion couples between Ni-based superalloys and pure Ni with high temperature aging are used to determine if there is a need to correct mobility of individual components or scale with a simple scaling factor (D_{scale}) to the calculated diffusivity from databases. Ultimately, XRD (X-Ray Diffraction) can be used to evaluate the importance of misfit and modify the molar volume models if needed.

For material specific model parameters of precipitation kinetics, nonisothermal nucleation experiments using SSDTA (Single Sensor Differential Thermal Analysis, see later discussion) were identified to determine coherent γ' surface energy (σ_{coh}) and estimated elastic coherency energy (G_{el}). Next, later stage coarsening experiments and controlled cooling for subsolvus treated sample are used to determine the incoherent γ' surface energy (σ_{incoh}) and possible interfacial mobility term (M_o). Finally, TEM study can be used to determine the coherency transition size ($R_{coh \rightarrow incoh}$), and to assist the calculation

[3] http://www.thermocalc.com/Products/TCC.html
[4] http://www.thermocalc.com/Products/Dictra.html

of elastic coherency energy (G_{el}). Additional details of experimental data development will be further discussed in following Sections.

Task 1 — Fundamental Multicomponent Models

Most of the technical activities of this Task were conducted during the 1st year of this program. Additional literature information appeared in the 2nd year, and thus, for completeness, the final results are provided here in this Section, which is separated into two Subsections: thermodynamics and diffusivity.

THERMODYNAMICS

To assess equilibrium phase fractions and compositions, water quenched supersolvus treated samples of ME3, LSHR, Alloy10 and RR1000 disc alloys are given 1000hr treatments at temperatures of 1093°C (2000°F), 927°C (1700°F), and 760°C (1400°F). Commercial thermodynamic databases compared in this study, using Thermo-Calc software, include Thermotech Ni-DATA versions 4 to 7[5], Computherm PanNickel[6], Ni-NIST[7] (not including Nb), and TCNI1[8] (not including Mo, Nb and Ta).

Alloy 10/ME3 Equilibrium Studies

Comparison in equilibrium phase compositions was undertaken with evaluation of the Alloy10 and ME3 samples quenched from the 1093°C 1000hr age treatment. The high-temperature matrix composition of ME3 was determined by both Energy Dispersive Spectroscopy (EDS) analysis conducted at NASA GRC and Atom-Probe Tomography (APT) using an Imago Local Electrode Atom Probe (LEAP) with new larger-FOV LEAP detector at the Northwestern University Center for Atom Probe Tomography (NUCAPT). In addition, γ' composition was also successfully measured by EDS for both alloys.

A LEAP dataset with 2.2 million atoms and dimensions of 36×37×60 nm^3 was analyzed for the ME3 sample. No large isothermally aged γ' was detected in LEAP (the fine γ' formed during quench will be discussed later), and thus the entire LEAP dataset represents the matrix during the high temperature age. Table 3 summarizes both the quantitative APT and semi-quantitative EDS results, and a comparison with the predicted high temperature matrix compositions using different thermodynamics databases. Based on the root mean square (RMS) error of solute content relative to the APT measurement, the Ni-DATA 7 database gives the best agreement. In the last column of Table 3, an experimental phase fraction of 24.8% was estimated by mass balance using the APT measured matrix composition and the Ni-DATA 7 predicted γ' composition, and again the Ni-DATA 7 prediction provides the best agreement. The comparison of predicted versus EDS measured γ' compositions also confirm the best agreement from the Ni-DATA 7 database. Based on these observations, ΔE (in Table 2) for Ni-DATA 7 7is thus taken to be zero in our simulation.

5 N. Saunders, M. Fahrmann and C.J. Small, "The Application of CALPHAD Calculations to Ni-Based Superalloys," Superalloys 2000, eds. K.A. Green, T.M. Pollock and R.D. Kissinger, (TMS, Warrendale, 2000), 803.
6 http://www.computherm.com/databases.html
7 Database provided by Dr. Ursula Kattner at NIST.
8 http://www.thermocalc.com/Products/Databases/TCNI1.htm

Table 3 Comparison of the predicted γ and γ' compositions and γ' phase fraction in ME3 at 1093°C (2000°F) with the experimental APT γ and EDS γ and γ' compositions. Ni-DATA version 5 (or 7) is abbreviated as Ni 5 (or 7) in the table.

		Composition at 1093°C, at%											γ' fraction
		Ni	Al	Cr	Co	Ti	Mo	W	Nb	Ta	C	RMS	
	APT	44.9	6.7	17.5	21.7	3.5	3.4	1.0	0.5	0.5	0.04		24.8
	2σ	0.04	0.02	0.03	0.03	0.01	0.01	0.01	0.01	0.01	0.002		1.5
	EDS	46.1	6.6	16.6	22.7	3.3	3.0	1.3*	0.6	-	-		
γ	Ni 5,6	45.7	5.6	19.7	22.1	2.4	3.1	0.7	0.3	0.3	0.01	0.93	30.7
	Ni 7	**46.4**	**6.0**	**18.5**	**21.8**	**2.7**	**3.0**	**0.7**	**0.4**	**0.5**	**0.01**	**0.54**	25.5
	Pan-Nickel	44.3	5.3	20.3	23.0	2.4	2.9	0.8	0.4	0.5	0.05	1.19	32.3
	NIST-Ni	44.7	5.1	19.9	23.8	2.4	3.2	0.8		0.2		1.44	29.4
	EDS	58.4	12.9	4.1	12.8	8.9	0.5	0.3	0.6	1.4	-		
	Ni 5,6	61.5	5.7	2.6	14.4	7.1	0.5	0.9	2.4	4.9	-	3.09	
γ'	**Ni 7**	**60.2**	**12.0**	**2.8**	**13.0**	**8.8**	**0.3**	**0.3**	**1.3**	**1.2**	**-**	**0.63**	
	Pan-Nickel	61.8	12.3	2.2	12.5	8.2	0.4	0.1	1.2	1.1	-	0.81	
	NIST-Ni	68.3	6.3	1.3	9.7	7.6	0.3	0.3	-	6.2	-	3.27	

* value includes both W and Ta due to peak overlaps in EDS.

High temperature γ and γ' compositions of Alloy 10 (1093°C 1000hr) were successfully measured by EDS, and compared with several thermodynamic databases in Table 4. Combined W+Ta composition is reported for EDS due to peak overlap. Overall, Ni-DATA 7 agrees the best with the semi-quantitative EDS measurement.

A systematic underestimation of Ti in the calculated γ matrix was also noted in QuesTek's earlier simulations in the DARPA-AIM initiative on commercial Ni-base superalloys and may have to be addressed later in this program.

Table 4 Comparison of the predicted γ and γ' compositions at 1093°C and EDS measurement for Alloy 10 aged at 1093°C for 1000 hr.

		Compositions, at%									
		Ni	Al	Cr	Co	Ti	Mo	W	Ta	Nb	RMS
	EDS	53.8	7.0	13.4	17.5	3.2	2.3	1.6		1.13	
γ	Ni 5,6	50.8	5.74	17.60	17.76	2.61	2.30	2.54	0.14	0.50	1.75
	Ni 7	**51.1**	**5.97**	**16.97**	**17.72**	**2.76**	**2.21**	**2.48**	**0.20**	**0.63**	**1.49**
	Ni-NIST	51.3	5.44	17.00	18.60	2.58	2.31	2.66	0.10	-	1.68
	EDS	62.3	13.0	4.0	10.9	7.2	0.6	0.9		1.3	
γ'	Ni 5,6	62.2	12.02	2.82	11.01	8.42	0.24	0.93	0.49	1.89	0.80
	Ni 7	**64.1**	**12.11**	**2.80**	**10.53**	**8.64**	**0.23**	**0.91**	**0.40**	**1.73**	**0.83**
	Ni-NIST	66.8	13.5	1.35	7.54	9.62	0.13	0.37	0.68	-	1.93

Ni-Al-Cr(-X) (X=Re,W) Model Alloys

Further comparison of thermodynamic databases is enabled by previous APT and ICP (Inductively Coupled Plasma atomic-emission spectroscopy measurement) studies at Northwestern University of isothermal γ' precipitation in simple Ni-Al-Cr-X model alloys. The measured time evolution of particle size suggests the precipitation composition trajectory can be modeled as an unstable equilibrium with capillarity. Comparison of phase compositions with the database predictions for these alloys is made in

Tables 5-8. For the base Ni-Al-Cr alloy at 600°C, measurement of the composition trajectory includes the initial critical nucleus composition. As metrics of relative impact of phase composition error, Tables 5-9 include not only the RMS solute concentration error and γ' phase fraction, but the corresponding predicted error in thermodynamically computed γ' APB enthalpy[9], and the at-temperature interphase lattice-parameter misfit based on QuesTek's molar volume model. These comparisons again support the Ni-DATA 7 database as most accurate, and suggest the corresponding error in APB enthalpy and misfit is acceptable within current structure/property model uncertainty.

While predicted phase fractions show good agreement with experiment for the complex superalloy of Table 3, we note a significant discrepancy for the simpler model alloys of Tables 5-8. For these alloys a ΔE shift in the relative free energy of γ' could be appropriate for further modeling of precipitation dynamics.

Table 5. Phase composition comparison of APT[10] and the database predictions for a Ni-5.2Al-14.2Cr (at%) alloy at 600°C

Ni-5.2Al-14.2Cr 600°C			at% Ni	Al	Cr	RMS	APB (J/m2)	600°C misfit %	% γ' fraction
γ	Equilibrium matrix composition	APT	81.26	3.13	15.61				
		2σ	0.18	0.08	0.18	0.14			
		Ni 5,6	81.40	3.64	14.96	0.58			
		Ni 7	**81.34**	**3.62**	**15.04**	**0.53**			
		TCNI1	81.17	3.93	14.90	0.76			
		Ni-NIST	80.60	5.20	14.20	1.77			
γ'	γ' equilibrium composition	APT	76.53	16.69	6.77		0.19	-0.7	15.4
		2σ	0.50	0.44	0.30	0.38	0.01		0.4
		Ni 5,6	74.98	16.23	8.80	1.47	0.19	-0.6	12.4
		Ni 7	**74.97**	**16.21**	**8.82**	**1.49**	0.19	-0.6	12.4
		TCNI1	75.59	14.55	9.57	2.49	0.18	-0.8	12.3
		Ni-NIST	75.96	12.25	11.79	4.74	0.15	-0.9	0.0
	Critical γ'-nucleus composition	APT	72.40	18.30	9.30		0.16	-0.2	
		2σ	2.20	1.80	1.40	1.61	0.03		
		Ni 5,6	74.91	17.37	7.71	1.30	0.20	-0.5	
		Ni 7	**74.91**	**17.40**	**7.69**	**1.30**	0.20	-0.5	
		TCNI1	75.36	16.43	8.21	1.53	0.20	-0.6	
		Ni-NIST	No precipitation						

[9] A.P. Miodownik and N. Saunders, Applications of Thermodynamics in the Synthesis and Processing of Materials, ed. Nash and Sundman, TMS, (1995) 91.

[10] C.K. Sudbrack, D. Isheim, R.D Noebe, N.S. Jacobson, and D.N. Seidman, "The Influence of Tungsten on the Chemical Composition of a Temporally Evolving Nanostructure of a Model Ni-Al-Cr Superalloy," *Microsc. Microanal*, 10 (2004), 355-365.

Table 6. Phase composition comparison of APT[11] and the database predictions for a Ni-7.5Al-8.5Cr (at%) alloy at 600°C

Ni-7.5Al-8.5Cr 600°C			at% Ni	Al	Cr	RMS	600°C misfit %	% γ' fraction
γ	Equilibrium matrix composition	APT	85.19	5.42	9.39			
		2σ	0.16	0.18	0.18	0.18		
		Ni5,6	85.71	5.42	8.86	0.37		
		Ni7	**85.71**	**5.42**	**8.86**	**0.37**		
		Ni-NIST	84.00	7.50	8.50	1.60		
γ'	γ' equilibrium composition	APT	76.33	17.82	5.85		-0.39%	16.1%
		2σ	0.24	0.30	0.24	0.27		0.3%
		Ni5,6	75.44	17.87	6.69	0.59	-0.26%	16.7%
		Ni7	**75.44**	**17.87**	**6.69**	**0.59**	-0.26%	16.7%
		Ni-NIST	76.38	16.37	7.25	1.42	-0.50%	0.0%
	Critical γ'-nucleus composition	APT	70.90	23.30	5.80		0.43%	
		2σ	2.80	3.00	1.80	2.47		
		Ni5,6	75.22	18.97	5.82	3.06	-0.19%	
		Ni7	**75.22**	**18.97**	**5.82**	**3.06**	-0.19%	
		Ni-NIST	No precipitation					

Table 7. Phase composition comparison of ICP[12] and the database predictions for a Ni-10Al-8.5Cr (at%) alloy at 800°C

800°C		at% Ni	Al	Cr	RMS	% γ' fraction
γ equilibrium matrix composition	ICP	82.71	8.43	8.86		
	2σ	0.24	0.16	0.18	0.17	
	Ni 5,6	82.93	8.32	8.75	0.11	
	Ni 7	**82.93**	**8.32**	**8.75**	**0.11**	
	Ni-NIST	81.90	9.76	8.34	1.01	
γ' equilibrium precipitate composition	ICP	76.60	17.41	5.99		14.6
	2σ	0.36	0.34	0.12	0.25	0.3
	Ni 5,6	75.52	18.64	5.84	0.88	13.9
	Ni 7	**75.52**	**18.64**	**5.84**	**0.88**	13.9
	Ni-NIST	76.47	17.40	6.13	0.10	0.0

[11] C. Booth-Morrison, J. Weninger, C. Sudbrack, Z. Mao, R. Noebe and D. Seidman, "Effects of solute concentrations on kinetic pathways in Ni–Al–Cr alloys," *Acta Materialia*, 56 (2008) 3422-3438.

[12] C.K. Sudbrack, T.D. Ziebell, R.D. Noebe, D.N. Seidman, "Effects of a tungsten addition on the morphological evolution, spatial correlations and temporal evolution of a model Ni–Al–Cr superalloy," *Acta Materialia*, 56 (2008) 448-463.

Table 8. Phase composition comparison of APT[13] and the database predictions for a Ni-Al-Cr-Re alloy at 800°C

800°C			at%					APB	800°C	% γ'
			Ni	Cr	Al	Re	RMS	(J/m2)	misfit %	fraction
γ	Equilibrium matrix composition	APT	81.07	10.04	6.74	2.15				
		2σ	0.16	0.04	0.08	0.02	0.05			
		Ni 7	**80.55**	**8.94**	**8.35**	**2.16**	**1.13**			
		Ni-NIST	80.22	8.79	8.87	2.12	1.42			
γ'	Equilibrium composition	APT	76.17	4.97	18.05	0.81		0.19	-0.71	24.8
		2σ	0.26	0.10	0.18	0.04	0.12	0.00		0.2
		Ni7	**75.29**	**5.68**	**18.80**	**0.23**	**0.68**	0.20	-0.68	15.9
		Ni-NIST	75.82	6.13	17.65	0.39	0.75		-0.77	7.2
	composition at 80% completion	APT	76.33	5.46	16.92	1.29		0.17		20.3
		2σ	0.30	0.16	0.26	0.08	0.18	0.00		0.2
		Ni7	**75.22**	**5.56**	**18.99**	**0.23**	**1.35**	0.20		12.8

Table 9. Phase composition comparison of APT[14] and the database predictions for a Ni-Al-Cr-W alloy at 800°C

800°C		at%					APB	800°C	% γ'
		Ni	Cr	Al	W	RMS	(J/m2)	misfit %	fraction
γ equilibrium matrix composition	APT	81.31	5.83	11.52	1.34				
	2σ	0.07	0.04	0.05	0.02	0.04			
	Ni7	**81.44**	**6.22**	**10.53**	**1.80**	**0.67**			
	Ni-NIST	80.48	8.57	8.84	2.11	2.26			
. γ' equilibrium precipitate composition	APT	76.30	17.00	3.91	2.80		0.21	-0.49	37.9
	2σ	0.08	0.07	0.04	0.03	0.05	0.00		0.0
	Ni7	**75.39**	**18.00**	**4.20**	**2.42**	**0.64**	0.22	-0.36	32.1
	Ni-NIST	75.87	16.61	6.42	1.09	1.77		-0.61	18.7

γ/γ' Lattice Misfit

Presence of γ/γ' lattice misfit introduces coherent misfit energy and alter the equilibrium compositions and fraction. In addition, the misfit energy in Ni-based superalloys changes the randomly distribution γ' particle into aligned cuboidal morphology. Figure 2 compares the γ' microstructures of supersolvus treated (1193°C/1hr) Alloy10 and RR1000 after long-term aging at 1093°C for 1000 hr. While the fine intragranular precipitates in Alloy10 show the cuboidal morphology and ordered arrays, indicating higher misfit, the γ' in RR1000 shows a spheroidal morphology and disordered spatial distribution. This observation is consistent with QuesTek preliminary γ/γ' lattice parameter model, which predicted LSHR having the highest misfit among the four, followed by Alloy10, ME3 and RR1000. However, JMatPro software[15] predicts low 0.2% or less lattice misfit for all four 3rd generation disc alloys studies here, suggesting lattice misfit is supposed to have minimum impact. To clarify this discrepancy, LSHR was selected for experimental XRD (X-ray Diffraction) lattice misfit study.

[13] C.K. Sudbrack, R.D. Noebe, and D.N. Seidman, "Compositional pathways and capillary effects during isothermal precipitation in a nondilute Ni-Al-Cr alloy," *Acta Materialia*, 55 (2007), 119-130.

[14] K.E. Yoon, R.D. Noebe, and D.N. Seidman, "Effects of rhenium addition on the temporal evolution of the nanostructure and chemistry of a model Ni–Cr–Al superalloy. II: Analysis of the coarsening behavior," *Acta Materialia*, 55 (2007), 1145-1157.

[15] http://www.thermotech.co.uk/jmatpro.html

(a) 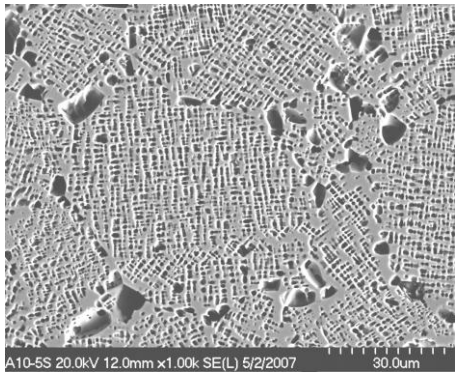

(b) 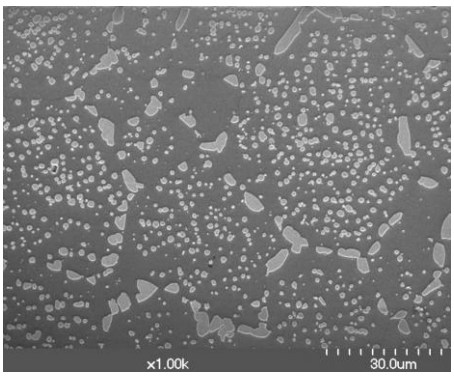

Figure 2. Comparison of the γ' microstructures of (a) Alloy 10 and (b) RR1000 (courtesy of L. Birrell at University of Cambridge)

NASA GRC conducted room temperature XRD experiments on two LSHR samples. They received different heat treatment and subsequent cooling to produce fine and coarse γ' microstructure. Figure 3 shows the representative γ' microstructure of the two samples. The γ/γ' lattice misfit was determined to be between 0.1~0.15%, compatible with JMatPro predictions. According to elastic micromechanics theory, the coherent misfit energy corresponding to this low level of misfit is negligible comparing to the chemical free energy. However, this low level of misfit might still be enough to produce ordered cuboidal morphology as seen in Figure 2a. Experimental determination of lattice misfit at high temperature relevant to γ' precipitation is ongoing at NASA GRC. With the information we have so far, the coherency misfit effects are ignored in our *PrecipiCalc* simulations. That is, G_{el} in Table 2 is taken to be 0.

(a) 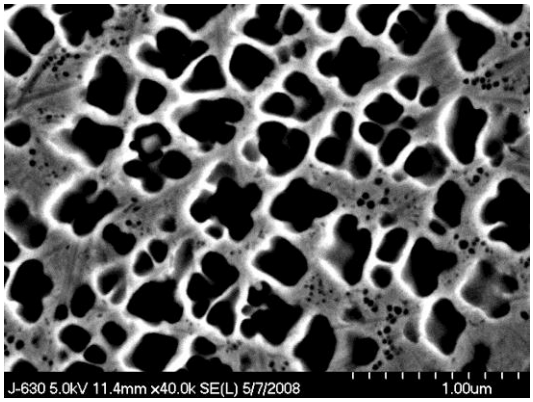

(b) 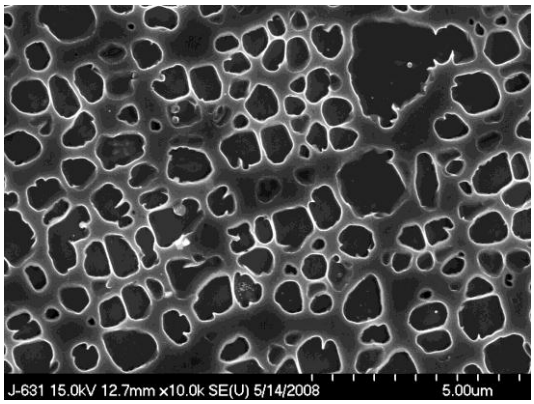

Figure 3 Two LSHR samples used for XRD lattice parameter and lattice misfit evaluation. (a) 2140F/1hr/air cooled, γ/ γ' lattice mismatch was found to be 0.1%; (b) 2100F/48hr/furnace controlled linear cooled (2100F to 1200F in 24hr), lattice mismatch was found to be 0.15%.

MOBILITY

To assess accuracy of available atomic mobility databases for combination with thermodynamic databases in order to predict multicomponent diffusivities, a linear diffusion "multiple" was prepared at NASA GRC[16]. A 5mm (0.2-inch) thick disc of pure Ni was diffusion bonded by hot pressing to a 3.2mm (0.125-inch) thick disc of ME3 on one side and to a 3.2mm (0.125-inch) thick disc of Alloy 10 on the other, for 4 hours at 877°C (1610 ºF) in vacuum. After the initial bond was formed, the diffusion couple was subjected to additional annealing in a horizontal tube furnace in an argon atmosphere at two temperatures, 1093°C or 927°C for 100 or 300 hours.

[16] Conducted by Dr. Ivan Locci at NASA GRC.

DICTRA simulations with Ni-DATA 7 and the NIST mobility database[17] of the diffusion multiple at the hot-pressing temperature 877°C predicted no significant diffusion. Therefore, subsequent simulations ignored the hot-pressing step.

Next, the NIST mobility database employed in the AIM project was compared with the Thermo-Calc MOB1 database in combination with various thermodynamic databases. In order to compare microprobe analyses of the diffusion multiple with DICTRA simulations, the average Matano interface (defined as the interface across which equal number of atoms have crossed in both directions) was equated to the origin of the calculated profiles, and simulations assumed that γ' precipitates act only as sink or source of solute for diffusion, i.e. no diffusion through γ'.

The agreement with the experimental microanalysis results is best using Ni-DATA 7 and NIST mobility databases. However, there are two discrepancies: (1) with the exception of Al, the experimental data does not confirm the predicted strong nonmonotonic profiles near the interface, and (2) the actual diffusion of Nb, Ta, Al, and Ti is less than predicted. Using the NIST mobility database with minor adjustments to the diffusivity prefactors of Cr, Nb and Ti (by factors of 1.4, 0.53 and 0.70, respectively), the predicted DICTRA composition profiles agree reasonably well with the microanalysis, as shown in two of the selected examples in Figure 4. However, comparative simulations reveals that these adjustments do not affect the γ' precipitation simulation with *PrecipiCalc*. Hence, we conclude there is no correction needed to the NIST mobility database and thus D_{scale} (see Table 2) is set to 1.

Furthermore, as seen in the micrograph of Figure 5(b), the width of significant grain growth in ME3 due to MC/γ' dissolution also agrees well with the DICTRA predicted phase fraction distribution in Figure 5(a).

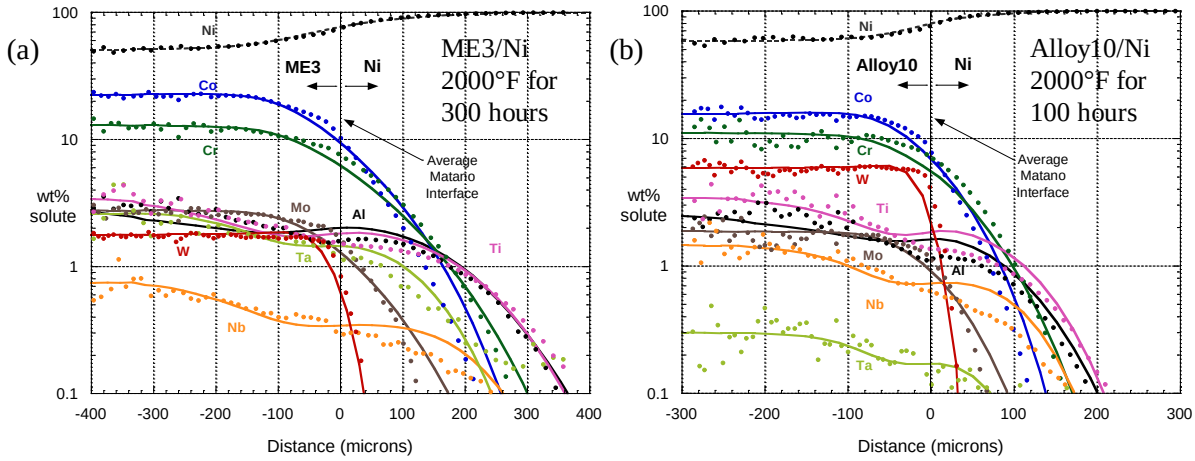

Figure 4. Comparison of microanalysis (discrete points) and composition trace predicted by DICTRA (curves) of (a) ME3/Ni diffusion couple aged at 1093°C (2000°F) for 300 hours, and (b) Alloy10/Ni diffusion couples aged at 1093°C (2000°F) for 100 hours

[17] C.E. Campbell, W.J. Boettinger, and U.R. Kattner, *Acta Materialia*, 50 (2002) 775-792.

(a)

(b)

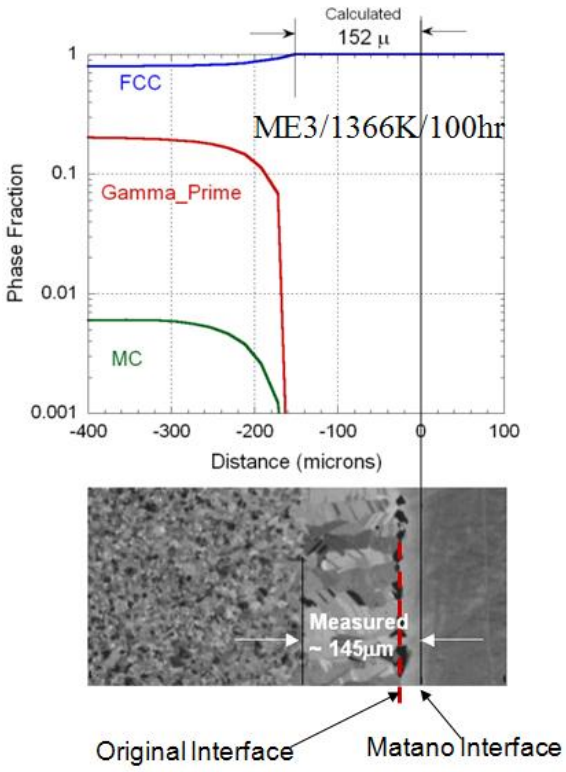

Figure 5. Comparison of (a) predicted equilibrium phase fractions, and (b) measured phase boundaries with adjusted Matano interface, for ME3/Ni 1093°C (2000°F)/100 hour diffusion multiple sample

Task 3 — γ' Precipitation Modeling

NUCLEATION ONSET TEMPERATURES AND SSDTA

As an efficient experimental check of nucleation behavior, transformation onset temperatures were measured in rapidly cooled arc melted samples of ME3 and Alloy10 using a Single-Sensor Differential Thermal Analysis (SSDTA) technique developed at Ohio State University[18]. From nucleation theory, the most important material parameters affecting the nucleation rate are driving force (which is determined by the bulk thermodynamics), surface energy and elastic coherency energy. Utilizing the SSDTA, we calibrated the surface energy, while initially ignoring the coherency elastic energy.

The transformation onset temperatures (T_{onset}) from the SSDTA experiments were determined from SSDTA data processing software, which takes the measured temperature versus time, fits the baseline prior to the transformation with a choice of function suitable for describing cooling, and then determines the departure point of measured data from the fitted function. The calibration of the SSDTA thermocouples has shown an accuracy of ±4.5°C [16] in the relevant temperature range. To determine the onset temperature from *PrecipiCalc* simulation with physically equivalent interpretation as closely as possible to the SSDTA results, the following summarizes our procedure.

[18] B.T. Alexandrov and J.C. Lippold, "Single Sensor Differential Thermal Analysis of Phase Transformations and Structural Changes during Welding and Postweld Heat Treatment," *Welding in the World*, 51, 11/12 (2007) 48-59 (Doc. IIW 1843-07).

- Process SSDTA measured temperature profiles to remove the latent heat contribution;
- Calculate material compositions relevant to the γ' precipitation from matrix γ phase — the high temperature phases (borides, carbides and undissolved γ') are removed with equilibrium calculations at highest SSDTA measured temperatures using the Ni-DATA 7 database.
- Perform *PrecipiCalc* simulations using Ni-DATA 7 and NIST mobility databases, with estimated surface energy;
- Collect time (or temperature) evolution results of γ' volume fraction (see Figure 6a), and compositions of matrix and γ', compute the time (or temperature) evolution of molar enthalpy (see Figure 6b);
- Compute temperature derivatives of the molar enthalpy with respect to temperature, dH/dT (see Figure 6c);
- Determine the transformation onset temperature where dH/dT changes by more than 10% of average dH/dT values, with decreasing temperature (see the vertical red dash line in Figure 6).

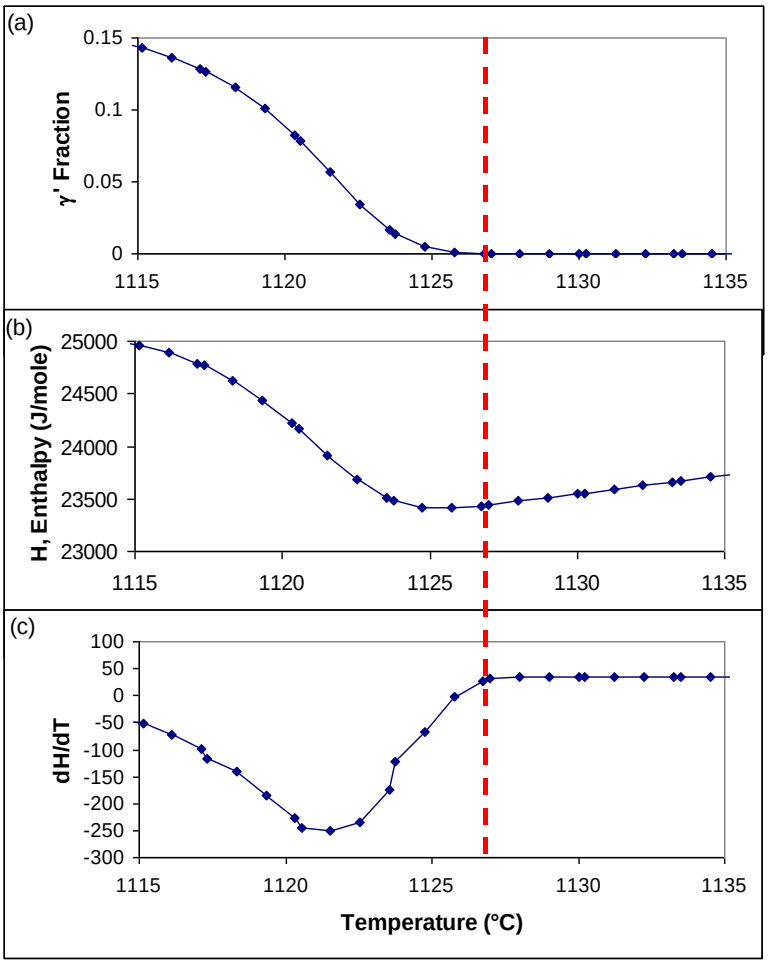

Figure 6 Determination of T_{onset} from *PrecipiCalc* simulations.

We note the difference of calculated T_{onset} values with the above enthalpy change approach and a simple approach of using a small γ' volume fraction of 0.1% is within the SSDTA accuracy.

Figure 7 summarizes the *PrecipiCalc* predictions with calibrated surface energy and compares the predictions to the transformation onset temperatures determined from SSDTA. We varied the surface energy between 0.0225 and 0.0325 J/m^2. Figure 7 shows the best-fit results with minimum RMS variation between prediction and measurement. Except for LSHR (which will be further discussed later), the optimized surface energies of disc alloys are similar and in agreement with the value of interfacial energy reported by Sudbrack et al. for the Ni-Al-Cr model alloys, 0.022~0.023 J/m^2.

The experimental uncertainty of T_{onset} associated with SSDTA is represented by error bars in Figure 7. The *PrecipiCalc* predictions with optimized interfacial energy agree with SSDTA results well, and mostly fall within the experimental uncertainty. Note that the T_{onset} temperatures, both measured and predicted, do not monotonically decrease with the average cooling rate between 1125 to 1160°C. If the temperature followed linear cooling, T_{onset} should have decreased monotonically with higher cooling rate. The actual local temperature profile clearly affected the measured T_{onset}, and *PrecipiCalc* predictions capture the non-monotonic behavior very well.

Due to a furnace temperature limitation of the SSDTA experiment, Alloy10, having the highest predicted γ' solvus temperature, contains undissolved γ' as confirmed by SEM (Figure 7). The observed amount is in good agreement with predicted equilibrium γ' fraction at the highest sample temperature in the furnace. The calculated transformation onset temperature of Alloy10 presented in Figure 7 is based on the assumption that the undissolved γ' particles do not grow during quenching, allowing us to completely remove them from *PrecipiCalc* simulations. To test this assumption, we performed a simulation of Alloy10 allowing the undissolved γ' to grow during quenching, which resulted in a reduction of nucleation onset temperature by only 1.6°C. Hence, the assumption to remove undissolved γ' from the *PrecipiCalc* simulation of the Alloy 10 SSDTA specimen is reasonable.

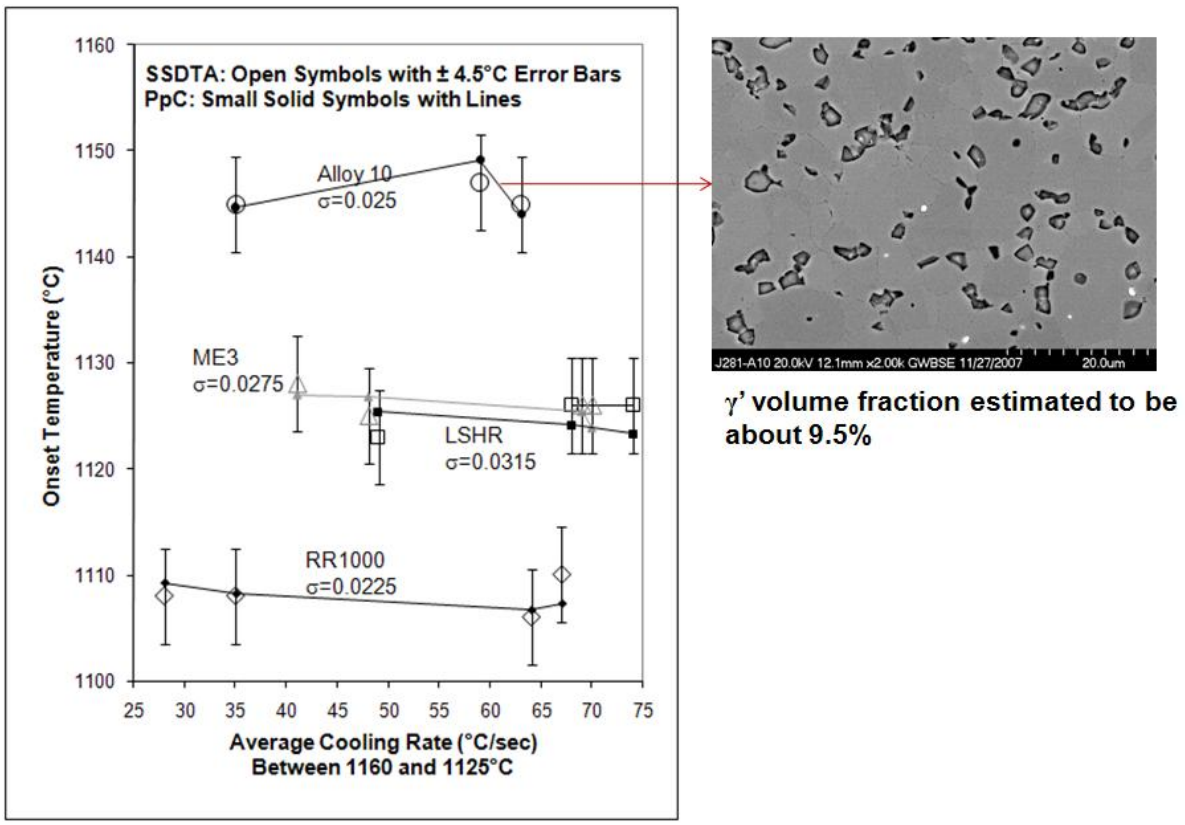

Figure 7. Summary of SSDTA results and *PrecipiCalc* (PpC) predictions with calibrated surface energy σ, in J/m^2

γ' MICROSTRUCTURE IN SSDTA SAMPLES

The well-defined thermal history of the SSDTA samples also provides an excellent opportunity for experimental validation of *PrecipiCalc* simulations of nonisothermal precipitation. Using LEAP APT, we analyzed the ME3 Ar gas-quenched sample (ME3-1Ar) from the SSDTA experiment. In total, 32 million atoms were analyzed. The overall bulk composition is very close to the expected composition. Larger γ' precipitates, about 40-60nm in diameter, were observed together with ultrafine γ' precipitates, about 5nm or less in diameter.

High-resolution SEM (HR SEM) analysis was also conducted on the same ME3-1Ar SSDTA sample, as well as an LSHR Ar gas-quenched sample (LSHR-2Ar). Consistent results between the APT and SEM for ME3-1Ar are shown in Figure 8. As shown by the higher magnification views at the bottom of Figure 8, fine γ' formed at lower temperature during SSDTA cooling was also observed in both ME3-1Ar LEAP APT and HR SEM.

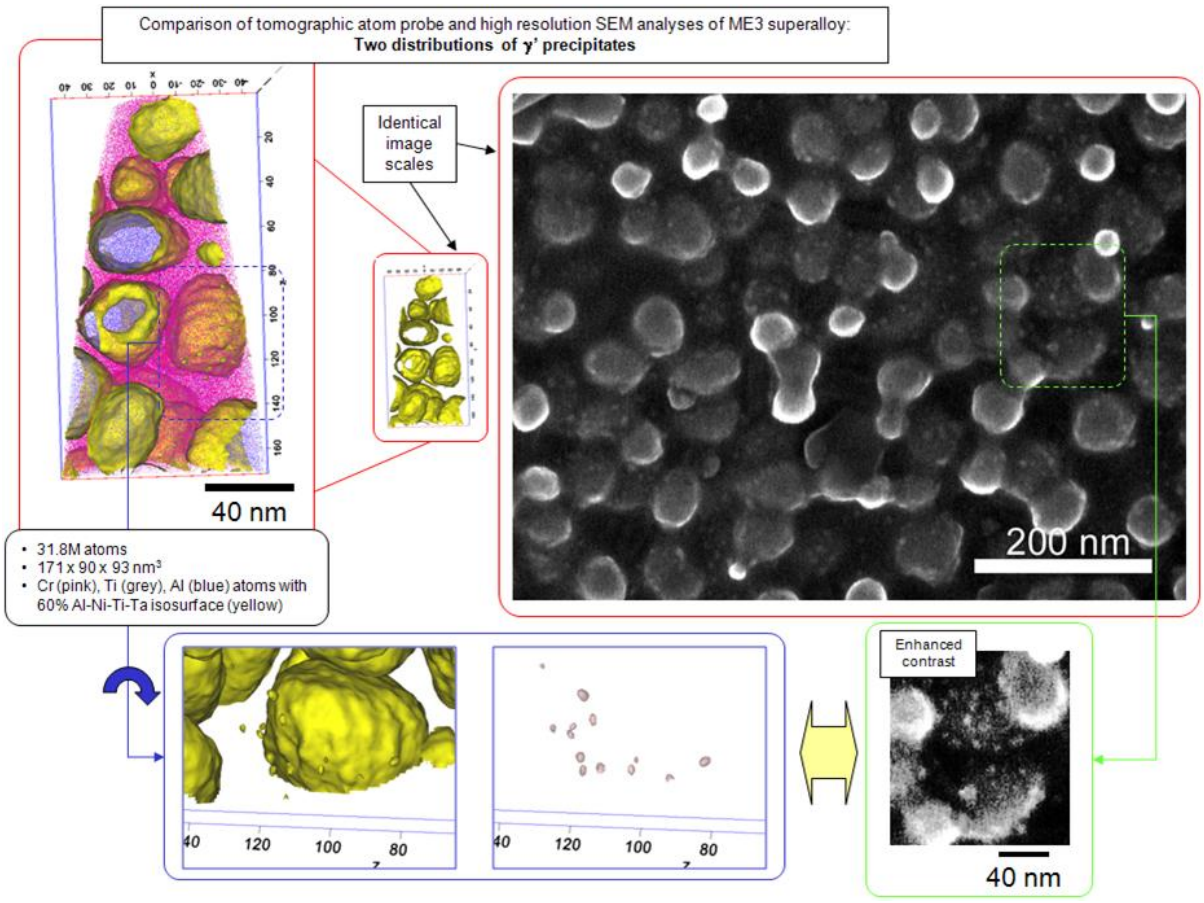

Figure 8. Characterization of γ' microstructure in an SSDTA specimen of ME3 quenched with Ar

Table 10 shows a summary of measured larger γ' size and also *PrecipiCalc* predictions using the measured SSDTA temperature profiles. *PrecipiCalc* provides reasonable estimates with the approximations employed thus far. Figure 9 shows reasonable agreement in particle size histograms between SEM and simulation for the SSDTA specimen of LSHR quenched with Ar. In the APT analysis of the SSDTA specimen of RR1000 quenched with He, the phase fraction of γ' was determined as about 35%, which agrees well with *PrecipiCalc*'s 37.6%.

Table 10. Comparison of the larger γ' mean diameter between two SSDTA samples and *PrecipiCalc* simulation using the surface energies discussed previously

	APT	SEM	*PrecipiCalc* Predictions
ME3-1Ar	40-60 nm	53.8 nm	41.0 nm
LSHR-2Ar	–	50.1 nm	45.6 nm
RR1000-3He	20-45 nm	31.8 nm	20.5 nm

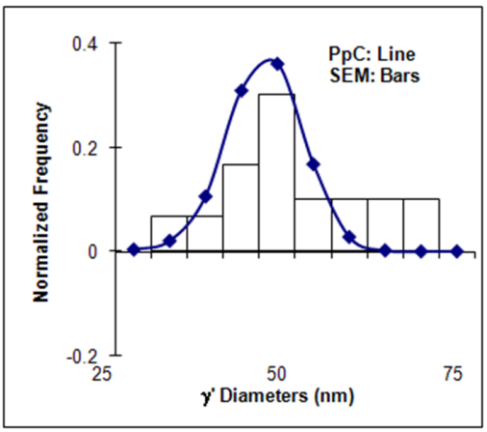

Figure 9. Comparison of particle size histogram from an SEM observation of 30 γ' particles and *PrecipiCalc* (3D results) simulation for an SSDTA specimen of LSHR quenched with Ar

Consistent with the thermodynamic prediction, the APT analysis of the SSDTA specimen of ME3 quenched with Ar shows that W partitions to the larger γ' phase. However, the W profile observed for the ultrafine γ' phase suggests that solute trapping of the slow-diffusing species may be occurring during precipitation at lower temperatures.

γ' MICROSTRUCTURE IN ME3 WATER QUENCHED SAMPLES

LEAP APT microanalysis was conducted on ME3 samples water quenched from both subsolvus treatment at 1093°C (1000hr) and supersolvus treatment at 1200°C (1hr). For the supersolvus treated sample, a LEAP dataset containing 8.7 million atoms within a box of 128×55×54 nm^3 was collected. The LEAP data analysis shows nanoscale γ' precipitates of about 15~30nm in diameter, which is in good agreement with our *PrecipiCalc* prediction of 30nm with an estimated cooling temperature profile. TEM work at NASA GRC indicates a larger mean diameter of γ' at 44nm.

For the 1093°C subsolvus treated ME3, the LEAP experiment used to obtain 1093°C matrix composition (Table 11) was further analyzed for fine quench γ'. An estimated 10-20nm effective diameter from LEAP APT is in reasonable agreement with the predicted 29nm diameter from *PrecipiCalc* simulation with an estimated cooling temperature profile. A proximity histogram of the subsolvus LEAP sample summarizes the measured partitioning of solutes between the γ and γ' phases in Figure 10. As summarized in Table 11 for both subsolvus and supersolvus treated samples, the partitioning is again in the direction of thermodynamic prediction, with the notable exception of the flat W profile offering further evidence that the slowest diffusing component exhibits solute trapping at extreme cooling conditions. Further study will address whether solute trapping need be considered for industrially-relevant processing conditions.

Table 11. Comparison of measured nanoscale γ' particle and matrix compositions in ME3 with corresponding *PrecipiCalc* simulations

ME3		Compositions, at%									
		Ni	Al	Cr	Co	Ti	Mo	W	Nb	Ta	RMS
Subsolvus											
γ	APT	42.5	4.9	21.3	23.7	2.3	3.6	1.0	0.4	0.3	
	PpC	35.0	2.82	27.3	27.7	0.51	5.28	1.30	0.07	0.08	2.80
γ'	ATP	55.6	9.3	7.3	17.5	6.1	2.1	0.8	0.4	0.8	
	PpC	61.3	12.8	2.1	12.2	8.2	0.42	0.52	1.2	1.2	3.07
Supersolvus											
γ	APT	40.5	4.8	22.5	23.8	2.0	4.2	0.8	0.6	0.5	
	PpC	39.2	3.00	24.6	27.5	0.74	3.94	0.87	0.08	0.13	1.71
γ'	APT	56.5	12.0	3.5	13.6	8.9	1.9	0.5	1.0	1.6	
	PpC	62.2	12.4	1.94	11.9	8.50	0.32	0.34	1.0	1.3	1.01

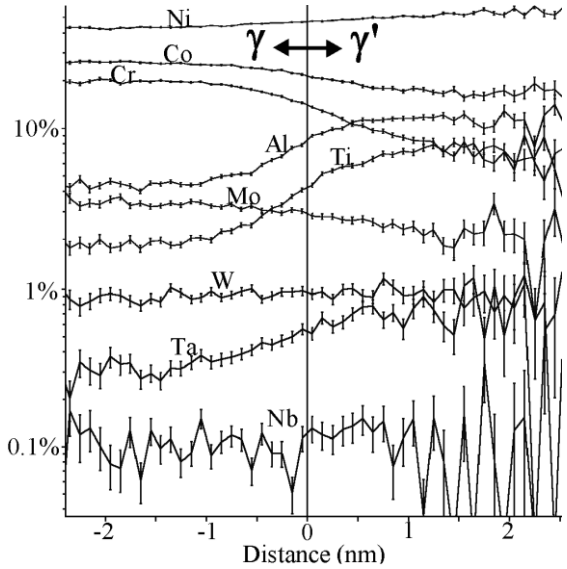

Figure 10. γ and fine quench γ' compositions (in atomic %) analysis of LEAP experiment on ME3 1093°C/1000-hour isothermal hold sample

γ' MICROSTRUCTURE IN FURNACE COOLED SAMPLES AFTER SUPERSOLVUS TREATMENT

To calibrate the interfacial mobility in a growth-dominated condition, we conducted furnace cooling on supersolvus-treated ME3, LSHR and Alloy10 specimens. Interfacial dissipation should be considered if *PrecipiCalc* predicts an overgrowth of γ' during the cooling after the subsolvus treatment. The cooling rate between 1160 and 1125 °C was around 0.54°C/second, about two orders of magnitude slower than the SSDTA experiment or water quenching. We measured the diameter of the γ' particles with SEM and compared the result to *PrecipiCalc* simulations. The simulations used the surface energies determined from SSDTA and the individually measured temperature cooling profile for each sample. The 3-dimensional results of *PrecipiCalc* were then converted to 2-dimensional numbers. Unlike the finer γ' particles formed during SSDTA fast cooling (see Figure 9) which were etched to reveal the 3-dimensional size in SEM, γ' particles here are much larger and should be compared to the 2-dimensional results. The 2-dimensional *PrecipiCalc* results are in a reasonable agreement with the SEM results, as shown in Table 12. Figure 11 further shows reasonable agreement between measured

particle size distribution and the simulation for the supercritical γ' particles in growth. The good agreements in mean diameter and particle size distribution suggest that interfacial dissipation can be neglected, at least for particle diameter up to about 500 nm.

Table 12. Comparison of the γ' mean diameter measured from SEM and *PrecipiCalc* simulations in furnace-cooled samples

	SEM	*PrecipiCalc* results converted to 2D
ME3	430 nm	348 nm
LSHR	408 nm	402 nm
Alloy 10	376 nm	396 nm

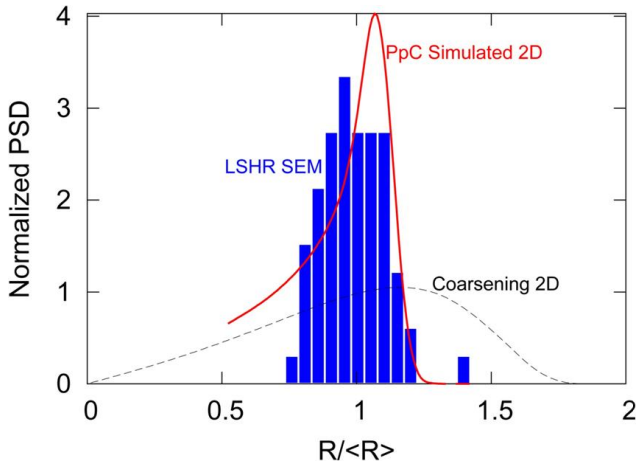

Figure 11. Comparison of particle size histogram from SEM and *PrecipiCalc* simulation converted to 2D (solid line) for a furnace-cooled sample of LSHR

Figure 12 compares the *PrecipiCalc*-simulated temperature dependency of mean radius, growth rate, ratio of mean radius over critical radius, and phase fraction of γ' in LSHR specimens furnace-cooled or quenched with Ar in SSDTA. Although at two very distinct cooling rates, γ' nucleates in a similar size within a narrow temperature window (1140~1142°C). Compared to the fast-cooled specimen in SSDTA, γ' particles at the slower cooling rate in the furnace show a slower growth rate below 1130°C (Figure 12(b)), due to a lower supersaturation. Nonetheless, γ' particles nucleated at the slower cooling rate in the furnace can grow to a much larger size relative to the critical size (Figure 12(c)). It is this dominance of growth that leads to the sharper size distribution of Figure 11.

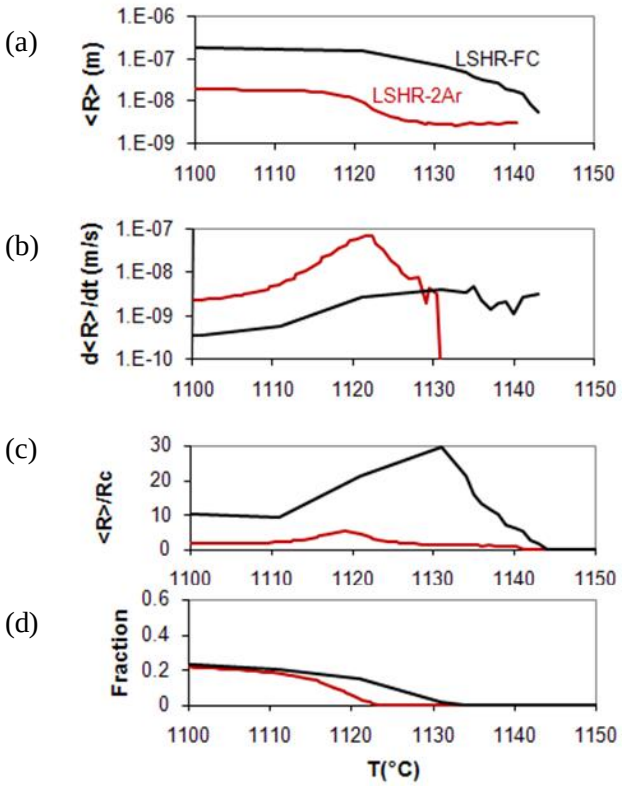

Figure 12. Comparison of *PrecipiCalc*-simulated temperature dependency of (a) mean radius (<R>), (b) growth rate, (c) ratio of mean radius over critical radius (R_C), and (d) phase fraction of γ' in LSHR specimens furnace-cooled (FC) or quenched with Ar in SSDTA (2Ar)

ISOTHERMAL COARSENING γ' MICROSTRUCTURE

We further calibrated *PrecipiCalc* based on coarsening data isothermally aged at high temperature. The goal of this set of experiments is to determine σ_{incooh} and M_o, as discussed in Table 2. In the previous subsection, we have shown that interfacial dissipation parameter M_o can assume infinity for γ' up to 0.5μm in diameter. The question is whether these two parameters will need to be considered for large incoherent particles.

The samples were analyzed under TEM or SEM, depending on the size of γ' particles. For higher temperature aging, both intragranular γ' and grain-boundary γ' particles are monitored as represented in Figure 13. Similar to Alloy 10 in Figure 2(a), the intragranular γ' in ME3 shows an ordered alignment, indicating a coherency-based elastic interaction. Eugine Kang, a student at Northwestern University, conducted image analysis at NASA GRC and measured the size and fraction of both intragranular γ' and grain-boundary γ' particles for ME3, LSHR, and Alloy 10. He then continued the analysis at Northwestern University on RR1000 alloy.

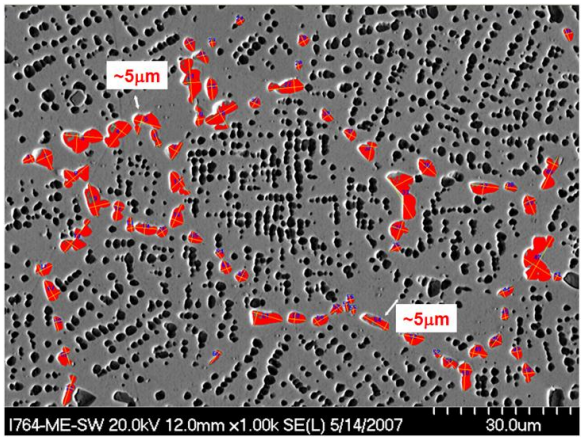

Figure 13. SEM image (processed to show intragranular and grain boundary γ' in black and grey, respectively) of ME3 supersolvus-treated and then aged at 1093°C (2000°F) for 1000 hours

Table 13 summarizes the measured γ' size at each aging condition. The grain-boundary γ' particles are typically larger than the intragranular γ' particles by a factor of about 1.5 to 2. Among ME3, LSHR, and Alloy 10, there is no consistent trend in the relative γ' size. We note that TEM measures the 3-dimensional size, while SEM measures the 2-dimensional size.

Table 13. Summary of measured γ' mean equivalent diameter (μm) of isothermally aged specimens.

Aging Conditions	Exp	ME3		LSHR		Alloy 10	
		Intragranular γ'	Grain-Boundary γ'	Intragranular γ'	Grain-Boundary γ'	Intragranular γ'	Grain-Boundary γ'
Before Aging	TEM	0.044	–	0.028	–	0.044	–
1093°C 5hr	SEM	0.298	0.412	0.312	0.446	0.306	0.486
1093°C 20hr	SEM	0.510	0.810	0.504	0.984	0.546	1.084
1093°C 100hr	SEM	0.739	1.500	0.720	1.324	0.808	1.566
1093°C 1000hr	SEM	1.380	2.840	1.420	2.996	0.894	2.618
927°C 1000hr	SEM	0.584	0.758	0.598	0.954	0.670	1.224
760°C 1000hr	TEM	0.058	–	0.062	–	0.062	–

Figure 14 compares the intragrain γ' size evolution at 1093°C aging of ME3 (solid green dots) with several simulation predictions (solid lines), to be discussed later. A $t^{1/3}$ type of coarsening equation (green text) describes the experimental data very well. In addition, experimental particle size distributions compare very well with the distribution from coarsening size distribution, see Figure 15. However, the fitted coarsening rate constant is a factor of 2~3 smaller than that predicted from theory. The *PrecipiCalc* simulation on intragrain γ' alone (without grain boundary γ'), using the surface energy determined earlier and non-zero volume correction factor, over-estimated the 1000hr size by a factor of 2. Note, we saw the same disagreement between the prediction and the experimental data for the other two alloys as well.

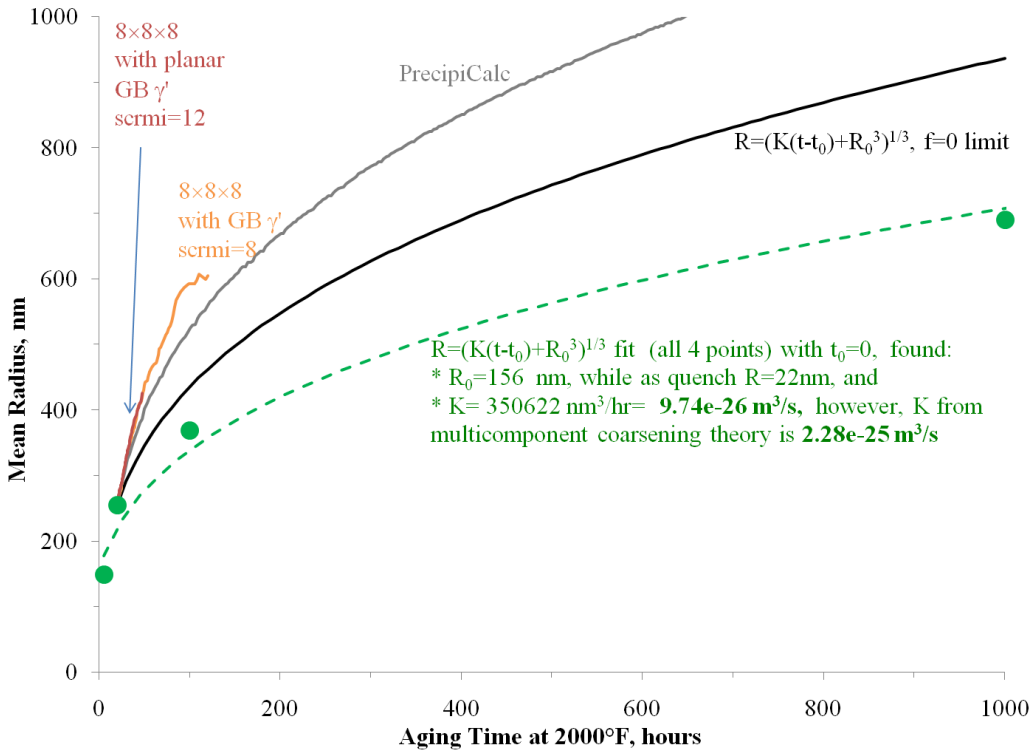

Figure 14 ME3 intragrain γ' mean size versus aging time. The four experimental data points are shown in green dots. Dashed curve represents the fit to the experimental data, and solid curves show various modeling prediction using 20hr as the starting condition.

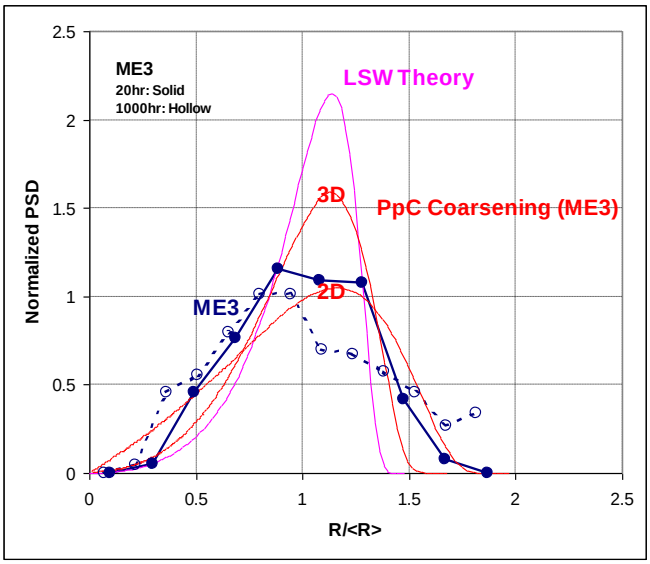

Figure 15 Comparison of normalized experimental ME3 intragrain γ' particle size distributions (1093°C for 20 and 1000hr) and several theoretical distributions, suggesting the particles are indeed evolving according to coarsening size distribution. Note the *PrecipiCalc* predicts broader size distribution than the LSW coarsening theory due to the non-zero volume fraction effects.

In an attempt to understand the slower than predicted coarsening rate, we surveyed the literature and found a rich body of research work. A quick summary of the literature includes:

- Misfit strain effect to coarsening[19] — 2D boundary integral simulation on elastically homogeneous precipitation system. Found (1) no effect on coarsening exponent, (2) no change in coarsening rate if particles maintain 4-fold symmetry, (3) coarsening rate increases for 2-fold symmetry. Similar conclusion in 3D by other researchers. The observed coarsening slowdown in this project is not predicted nor supported by these simulations.
- Trans-interface diffusion-controlled coarsening (TIDC)[20] — the semi-ordered diffuse interface around γ' could mean slower interfacial motion than predicted by volume diffusion alone. The theory predicts the impact occurs at small γ' size. Our experimental data shows fairly consistent coarsening behavior from 5hr to 1000hr. The TIDC mechanism doesn't seem to apply to our case here.
- Elastically inhomogeneous effects on coarsening[21] on isotropic system — multiscale consideration on both bulk and interfacial elasticity. Predicts coarsening slowdown at large particle sizes. This doesn't apply to our data either.
- Coherency transition — QuesTek studied M_2C in Ni-Co high strength steel using a combined misfit energy and surface energy transition across a critical particle size. The predicted M_2C coarsening shows a smaller exponent than 1/3, and compares very well with the experimental data. However, the intragrain γ' evolution follows the 1/3 exponent very well and doesn't seem to show the characteristics of coherency transition.

Another attempt to rationalize the slow coarsening behavior came from the consideration of both intragrain and grain boundary γ'. The large grain boundary particles are supercritical. With sufficient time, they can grow at the expense of the smaller intragrain particles. The question is, is the slow coarsening rate of intragrain γ' caused by the presence of the grain boundary γ'? To understand this, we employed the multipole expansion method. Similar to *PrecipiCalc*, the multipole expansion method solves the diffusion field explicitly, but it does so without the mean field assumption used in *PrecipiCalc*. Norio Akaiwa and Prof. Voorhees[22] at Northwestern University originally developed the multipole code in Fortran for binary systems, which is used here. Under the ONR/DARPA D3D program, we extended the formulation to multicomponent systems using a pseudobinary representation[23], which is also used here. Using this multipole software, we hope to quantify the impact of grain boundary γ' to the coarsening behavior of the intragrain γ'.

To setup the multipole simulation for ME3 at 1093°C (2000°F), we used an initial configuration from the experimental ME3 γ' microstructure at 1093°C/20hr from Table 13. The phase fraction of intragranular (grain boundary) γ' is about 19% (4%) from the image analysis. We utilized a simulation box sized $8\times8\times8$ μm^3 containing 1298 particles, 40 of which were the grain-boundary γ' particles represented at the planar array in red, see Figure 16. The remaining 1258 intragranular particles represented in green followed the LSW particle size distribution and were spatially random, so there is no PFZ (precipitate free zone) in the beginning of the simulation. For clarity, the particles in Figure 16 are shown smaller than actual size.

[19] K. Thornton, N. Akaiwa and P. Voorhees, *Phys. Rev. Let.*, 86 (7), (2001) 1259, and K. Thornton, N. Akaiwa and P. Voorhees, *Acta Mater.* 52 (2004) 1353-1364.
[20] A. Ardell and V. Ozolins, *Nature Materials* 4, (2005) 309.
[21] D. Perez and L. Lewis, *Phys. Rev. E*., 74, 031609 (2006), and D. Perez and L. Lewis, *Phys. Rev. E*., 75, 041602 (2007).
[22] N. Akaiwa and P. Voorhees, *Phys. Rev. E*., 49 (5), (1994) 3860.
[23] S. Farjami, P. Voorhees, S. Roper and H.-J. Jou, "Multiparticle Growth and Coarsening," presented in ONR/DARPA D3D review meeting, September 9, 2008, Columbus, OH.

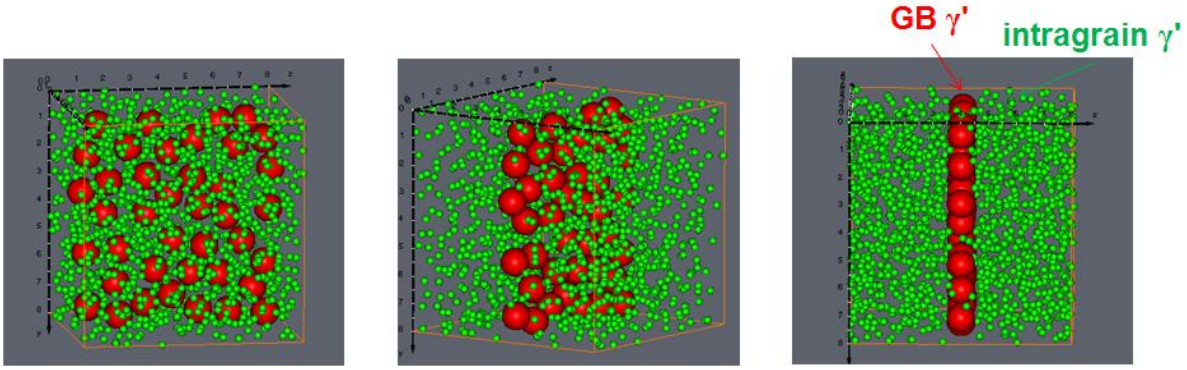

Figure 16. Initial configuration for the multipole simulation of ME3 for 20hr condition. The intragrain γ' are shown smaller in order to illustrate the configuration of two distribution of γ' particles.

The simulation result for ME3 aged at 1093°C (2000°F) for 48 hours shows 277 particles left, as shown in Figure 17. There are 40 grain-boundary γ' particles with a mean diameter of 1.3 μm. The phase fraction of these grain-boundary γ' particles after aging for 48 hours is about 8%, inconsistent with the measured phase fraction for a longer aging time – about 5% at 1000 hours from Figure 13. Nonetheless, the multipole simulation successfully captured the development of PFZ. The remaining 237 intragranular particles show a mean diameter of 0.79 μ with a phase fraction of about 15%.

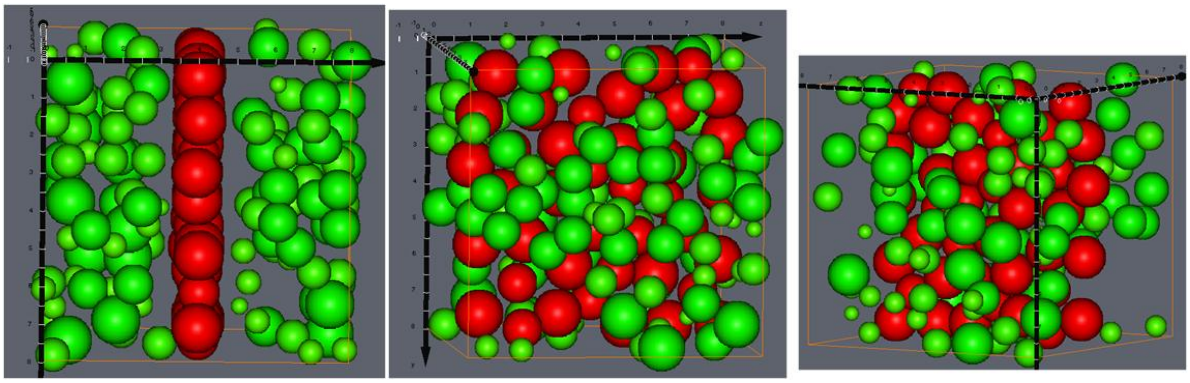

Figure 17. Multipole simulation of ME3 aged at 1093°C (2000°F) for 48 hours

Interestingly, the mean size evolution of intragrain γ' from the multipole simulation is in good agreement with our earlier *PrecipiCalc* simulation which did not consider grain-boundary γ' particles. Therefore, the size evolution of intragranular γ' particles does not seem to be affected by the presence of grain-boundary γ' particles. Figure 14 shows the multipole simulated intragrain γ' in dark brown[24] lines and the *PrecipiCalc* simulation in grey. The influence of grain boundary γ' to intragrain γ' is localized (only the intragrain γ' near grain boundary γ' are affected), so the overall mean size behavior of intragrain is not affected. Hence, we concluded the grain boundary γ' is not the source of intragrain γ' coarsening slowdown.

[24] There is another multipole simulation, shown with orange curve, with one single grain boundary γ' at the center of the box. More departure from *PrecipiCalc* simulation as particles get larger could be due to the reduction in number of particles in the multipole simulation, resulting in lack of accuracy.

However, given that aging at 1093°C (2000°F), let alone for 1000 hours, is not relevant to industrial aging practices, we decided to shelve further modeling activities to resolve the model discrepancy. Determination of incoherent surface energy and interfacial dissipation will be determined with the next set of experiments.

PRIMARY γ' MICROSTRUCTURE IN SUBSOLVUS SOLUTION TREATED LSHR

Another set of experiments focusing on primary γ' were developed to calibrate σ_{incoh} and M_o terms for *PrecipiCalc*. Two LSHR samples were subsolvus solution treated at 1145°C for 1 hour by NASA GRC, followed by either water quench or furnace controlled cool (at 60°F/min cooling rate). The resulting primary γ' microstructure is summarized in Figure 18. The *PrecipiCalc* simulation will be established in the third year of the project to determine both σ_{incoh} and M_o terms for large incoherent γ' particles.

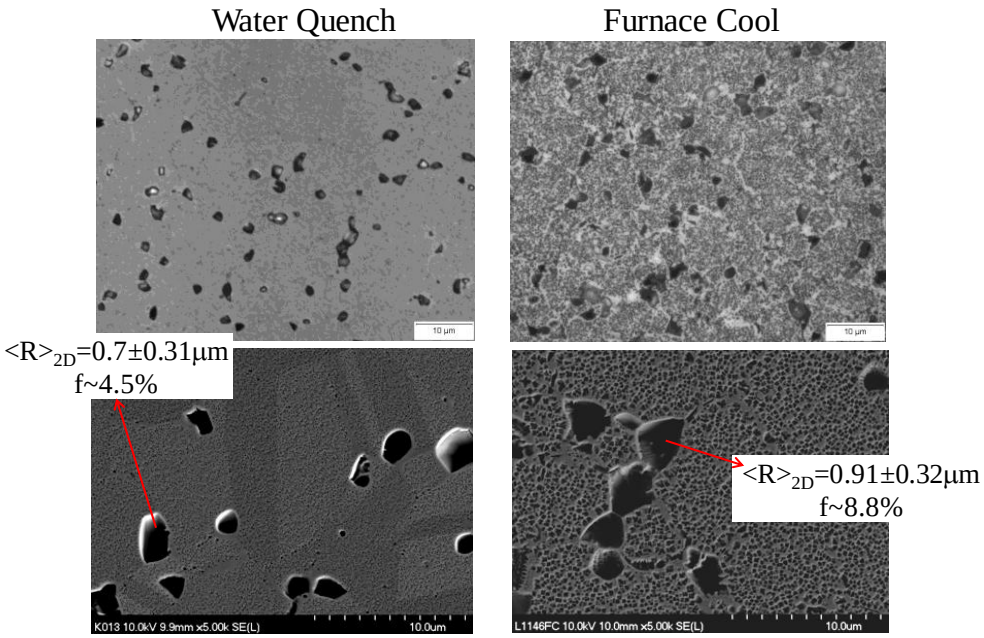

Figure 18 Micrographs observation (by NASA GRC) of LSHR 1145°C/1hr subsolvus solution treatment followed by two cooling paths.

Task 5 — Software Implementation and Dissemination

Though *PrecipiCalc* has shown to be an accurate tool for capturing γ' microstructure (except the extremely long age at high temperature, as previously discussed) for industrial relevant heat treatment processes, there are hurdles to utilizing a single *PrecipiCalc* computation for the entire heat treatment cycle:

- Mean field assumption — the growth model in *PrecipiCalc* assumes that all particles interact through a common mean field composition. This over-estimates the coarsening behavior of multimodal distributions — distribution with a larger size grows too fast at the expense of the smaller size distribution. For example, at the end of an aging *PrecipiCalc* simulation with both secondary and tertiary γ', the tertiary γ' will be predicted to completely dissolve away, which is not correct. Under the DARPA AIM program, QuesTek developed a multistep *PrecipiCalc*

simulation scheme to artificially remove (freeze) the larger distribution and perform the simulation on the smaller distribution only. This approach was shown accurate for 3rd generation disc alloys as well, and will be further extended and implemented in this program.

- Thermo-Calc convergence in free energy minimization — in a high order multicomponent system involving several phases, free energy minimization for equilibrium involves complex and iterative numerical computations. If an energy minimization failed to converge (such as trapped at a local minimum), the phase compositions could be non-physical and thus cannot be used. The complexity of the problem is further exacerbated by *PrecipiCalc* as it uses Thermo-Calc to compute states at non-equilibrium conditions at low temperature away from phase boundaries, where database developers might not have fully tested the ease of convergence. Sometimes this convergence problem can be alleviated by utilizing better initial estimates (start conditions) for energy minimization. But there are cases where the convergence is simply very difficult to achieve within Thermo-Calc for particular calculations. An example is the combined MC carbide and γ' precipitation within FCC matrix during quench from subsolvus treatment temperature for LSHR alloy, where the Thermo-Calc API could not obtain the correct MC carbide compositions within *PrecipiCalc*'s non-equilibrium precipitation simulation.

Driven by the need to overcome the above two issues, and the desire to further develop *PrecipiCalc* as a useful precipitation simulation tool for aeroturbine disc material engineers, one major focus of the third (last) year of this project will be to develop a software tool that accomplishes the following objectives:

- Partitions the entire heat treatment cycle into several *PrecipiCalc* simulations to mitigate the mean field and energy minimization convergence issues discussed above;
- Automatically prepares proper input files for individual simulations and summarizes results (this will involve automatic mass balance among phases and phase region tracking) in order to avoid the human operation error;
- Provides simple graphical user interface of pre-/post-process the input/output to simplify and accelerate the calculation setup and output visualization;
- Maintains the linkage to software robot (like iSIGHT) to allow an automated large amount of process simulation.

To achieve the above objectives, we have established the software architecture as shown in Figure 19. There are two components of this software, discussed in detail below.

- Multistep *PrecipiCalc* wrapper:
  - Handles and implements all the partitioning necessary in space, time and phases, and sets up the multistep *PrecipiCalc* simulation path;
  - Activates individual *PrecipiCalc* computation and post-processing with text-based input and output;
  - Performs necessary mass balance and mass transport between different partitions;
  - Collects all results into a text file;
  - To be implemented in Python scripting language and will support multiple platforms;
  - Can be used by the graphical user interface discussed below or software robot like iSIGHT or DAKOTA. User will not directly operate this code.

- Graphical User Interface (GUI):
  - Input → Preprocessing Module;
  - Compute → Computing Module;
  - Plot → Postprocessing Module;
  - Provides user interaction to Multistep *PrecipiCalc* Wrapper code;
  - Provides postprocessing and visualization capability;
  - Supports multiple platforms with Java Swing and PLPlot scientific plotting library.

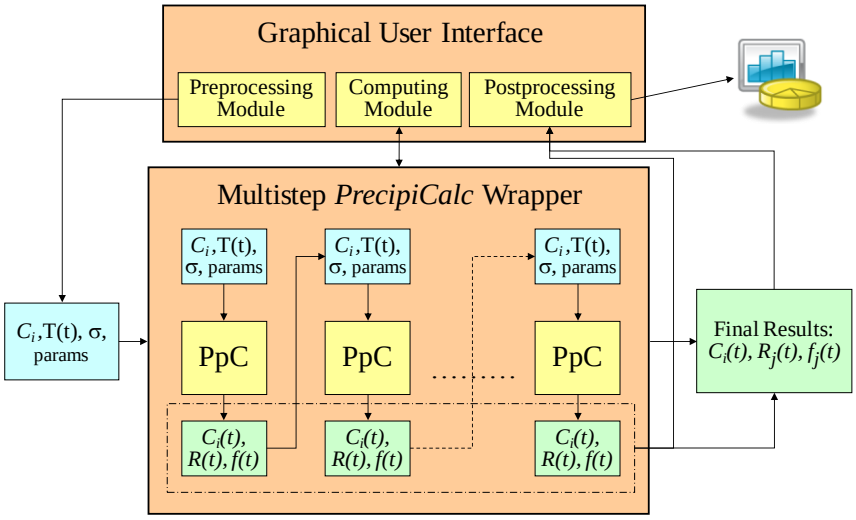

Figure 19 Software implementation structure for multistep *PrecipiCalc* (PpC) simulations for both subsolvus and supersolvus disk heat treatment. *C*, *T*, σ, *R* and *f* represent compositions, temperature, surface energy, mean size and volume fraction.

The multistep *PrecipiCalc* simulation breakdown for subsolvus and supersolvus heat treatment is summarized in Figure 20 and Figure 21, respectively. The decision to stop a *PrecipiCalc* calculation and then start a new simulation is determined by the two hurdles (mean field assumption and thermodynamics convergence) discussed in the beginning of this section. This approach differs from the method used in the DARPA AIM program in that (1) we include both carbide and γ' in the simulation, and (2) we allow controlled communication between large and small distributions during isothermal aging, instead of completely freezing and removing the large distribution. Further details will need to be determined in each simulation steps in the 3rd year of the project.

QuesTek is planning to complete a preliminary version of the software and distribute it to the project participants in the Spring of 2009.

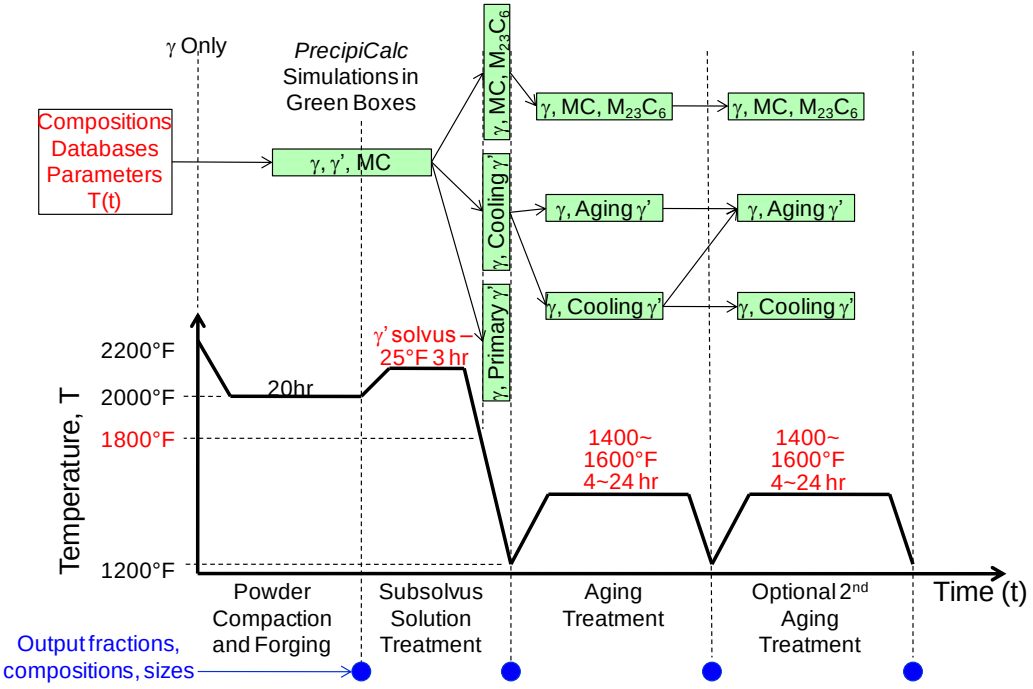

Figure 20 Detail breakdown of subsolvus disk heat treatment into several individual *PrecipiCalc* computations.

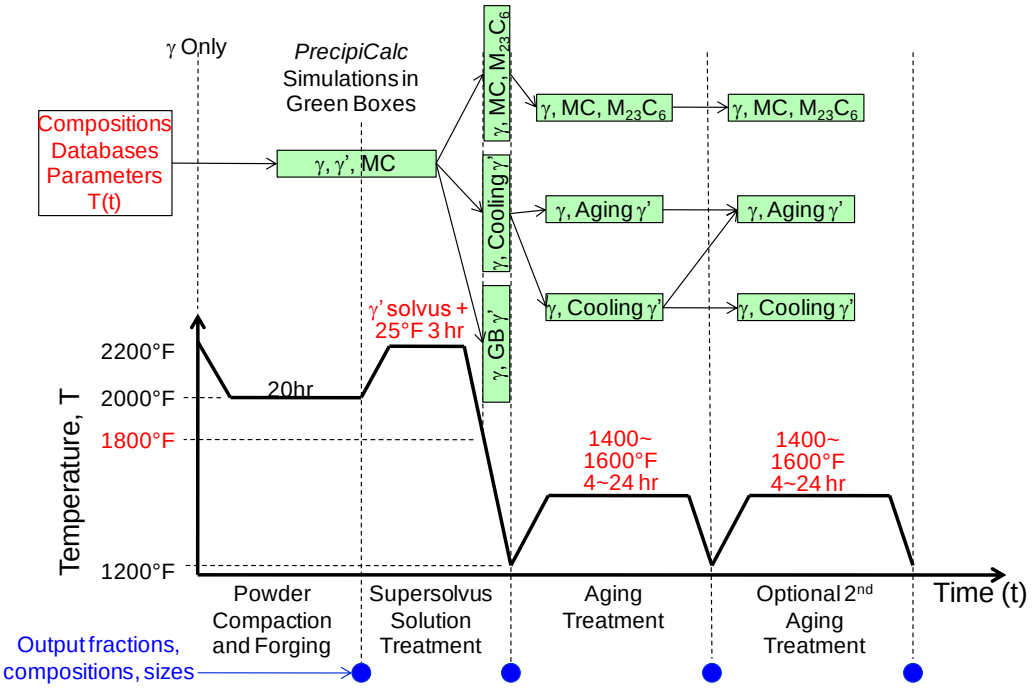

Figure 21 Schematic Detail breakdown of supersolvus disk heat treatment into several individual *PrecipiCalc* computations.

Conclusions and Next Steps

At the end of 2nd year of this NASA project, the status of each Task is summarized below.

- Task 1 Fundamental Multicomponent Models is completed successfully. No additional work is anticipated in this Task.
- Task 2 Development of Calibration and Validation Data — Development of γ' calibration data is mostly complete, and minor incomplete activities such as high temperature γ/γ' misfit will be completed in Year 3. The development of γ' validation data for industrial heat treatment cycle at NASA is nearly complete. Data of carbides microstructure will be further developed in Year 3.
- Task 3 γ' Precipitation Modeling — Completed most of the calibration, except the incoherent surface energy and interfacial dissipation parameters, which will be completed in Year 3. Except for the high temperature long term aging, *PrecipiCalc* has shown to accurately capture the precipitation microstructure in the 3rd generation disc alloys. The validation of the precipitation model against experiments with disc heat treatment cycle will be established in Year 3 of the project. (1st Objective of Year 3).
- Task 4 Precipitation Modeling for Embrittling Phases — Carbide modeling will be activated when experimental data is available in Year 3.
- Task 5 Software Implementation and Dissemination — The software implementation plan was established, and the software development is ongoing. The first dissemination to the team participants will be available in the Spring of 2009, and the final version will be distributed by the end of the project. (2nd Objective of Year 3).
- Task 6 Microstructure Variation and Optimization — Will be developed in Year 3.
- Task 7 Project Management and Reporting — In 2008, we have completed monthly reports, an article for the *Superalloys 2008* conference proceeding, and this 2nd annual report.

REPORT DOCUMENTATION PAGE		Form Approved OMB No. 0704-0188

1. REPORT DATE *(DD-MM-YYYY)*	2. REPORT TYPE	3. DATES COVERED *(From - To)*
01-03-2010	Final Contractor Report	

4. TITLE AND SUBTITLE
Microstructure Modeling of 3rd Generation Disk Alloys
Second Annual Report

5a. CONTRACT NUMBER
NNC07CB01C

5b. GRANT NUMBER

5c. PROGRAM ELEMENT NUMBER

6. AUTHOR(S)
Jou, Herng-Jeng

5d. PROJECT NUMBER

5e. TASK NUMBER

5f. WORK UNIT NUMBER
WBS 698259.02.07.03.04.02

7. PERFORMING ORGANIZATION NAME(S) AND ADDRESS(ES)
QuesTek Innovations LLC
1820 Ridge Avenue
Evanston, Illinois 60201

8. PERFORMING ORGANIZATION REPORT NUMBER
E-17216

9. SPONSORING/MONITORING AGENCY NAME(S) AND ADDRESS(ES)
National Aeronautics and Space Administration
Washington, DC 20546-0001

10. SPONSORING/MONITOR'S ACRONYM(S)
NASA

11. SPONSORING/MONITORING REPORT NUMBER
NASA/CR-2010-216229

12. DISTRIBUTION/AVAILABILITY STATEMENT
Unclassified-Unlimited
Subject Category: 07
Available electronically at http://gltrs.grc.nasa.gov
This publication is available from the NASA Center for AeroSpace Information, 443-757-5802

13. SUPPLEMENTARY NOTES

14. ABSTRACT
The objective of this program is to model, validate, and predict the precipitation microstructure evolution, using *PrecipiCalc* (QuesTek Innovations LLC) software, for 3rd generation Ni-based gas turbine disc superalloys during processing and service, with a set of logical and consistent experiments and characterizations. Furthermore, within this program, the originally research-oriented microstructure simulation tool will be further improved and implemented to be a useful and user-friendly engineering tool. In this report, the key accomplishment achieved during the second year (2008) of the program is summarized. The activities of this year include final selection of multicomponent thermodynamics and mobility databases, precipitate surface energy determination from nucleation experiment, multiscale comparison of predicted versus measured intragrain precipitation microstructure in quench samples showing good agreement, isothermal coarsening experiment and interaction of grain boundary and intergrain precipitates, primary γ' microstructure of subsolvus treatment, and finally the software implementation plan for the third year of the project. In the following year, the calibrated models and simulation tools will be validated against an independently developed experimental data set, with actual disc heat treatment process conditions. Furthermore, software integration and implementation will be developed to provide material engineers valuable information in order to optimize the processing of the 3rd generation gas turbine disc alloys.

15. SUBJECT TERMS
Gas turbine engines; Rotating disks; Heat resistant alloys

16. SECURITY CLASSIFICATION OF:			17. LIMITATION OF ABSTRACT	18. NUMBER OF PAGES	19a. NAME OF RESPONSIBLE PERSON
a. REPORT	b. ABSTRACT	c. THIS PAGE			STI Help Desk (email:help@sti.nasa.gov)
U	U	U	UU	36	19b. TELEPHONE NUMBER *(include area code)* 443-757-5802